The halo distribution of 2dF galaxies

Author(s):
Magliocchetti, Manuela; Porciani, Cristiano

The halo distribution of 2dF galaxies

Manuela Magliocchetti[1]* and Cristiano Porciani[2,3]

[1]*SISSA, Via Beirut 4, 34014, Trieste, Italy*
[2]*Institute of Astronomy, Madingley Road, Cambridge CB3 0HA*
[3]*Institut für Astronomie, HPF G3.2, ETH Hönggerberg, 8093 Zürich, Switzerland*

ABSTRACT

We use the clustering results obtained by Madgwick et al. (2003) for a sample of 96 791 galaxies from the 2dF Galaxy Redshift Survey with redshift $0.01 < z < 0.15$ to study the distribution of late-type and early-type galaxies within dark matter haloes of different mass. Within the framework of our models, galaxies of both classes are found to be as spatially concentrated as the dark matter within haloes, even though, while the distribution of star-forming galaxies can also allow for some steeper profiles, this is ruled out drastically in the case of early-type galaxies. We also find evidence for morphological segregation, as late-type galaxies appear to be distributed within haloes of mass-scales corresponding to groups and clusters up to about two virial radii, whereas passive objects show a preference to reside closer to the halo centre. If we assume a broken power law of the form $\langle N_{\rm gal}\rangle(m) = (m/m_0)^{\alpha_1}$ for $m_{\rm cut} \leqslant m < m_0$ and $\langle N_{\rm gal}\rangle(m) = (m/m_0)^{\alpha_2}$ at higher masses to describe the dependence of the average number of galaxies within haloes on the halo mass, fits to the data show that star-forming galaxies start appearing in haloes of masses $m_{\rm cut} \simeq 10^{11}\ {\rm M_\odot}$, much smaller than what is obtained for early-type galaxies ($m_{\rm cut} \simeq 10^{12.6}\ {\rm M_\odot}$). In the high-mass regime $m \geqslant m_0$, $\langle N_{\rm gal}\rangle$ increases with halo mass more slowly ($\alpha_2 \simeq 0.7$) in the case of late-type galaxies than for passive objects which present $\alpha_2 \simeq 1.1$. The above results imply that late-type galaxies dominate the 2dF counts at all mass-scales. We stress that – at variance with previous statements – there is no degeneracy in the determination of the best functional forms for $\rho(r)$ and $\langle N_{\rm gal}\rangle$, as they affect the behaviour of the galaxy–galaxy correlation function on different scales.

Key words: galaxies: fundamental parameters – galaxies: statistics – cosmology: observations – cosmology: theory – large-scale structure of Universe.

1 INTRODUCTION

Measurements of the galaxy–galaxy correlation function contain a wealth of information both on the underlying cosmological model and on the physical processes connected with the formation and evolution of galaxies. Untangling these two effects from the observed clustering signal of a particular class of sources is, however, not an easy task. For instance, the physics of galaxy formation affects the relationship between the distribution of luminous and dark matter (the so-called 'bias') so that different types of galaxies are expected to exhibit different clustering properties. Indeed, this has been observed (see, for example, Loveday et al. 1995; Guzzo et al. 1997; Loveday, Tresse & Maddox 1999; Magliocchetti et al. 2000, just to mention few) in the past decade, when large-area surveys started including enough sources to allow for precision clustering statistics.

From a theoretical point of view, the relationship between dark matter and galaxy distribution has not yet fully been understood, be-

cause although the dynamics of dark matter is only driven by gravity and is fully determined by the choice of an appropriate cosmological model (see, for example, Jenkins et al. 1998), the situation becomes increasingly difficult as one tries to model the physical processes playing a role in the process of galaxy formation.

As a first approximation, galaxies can be associated with the dark matter haloes in which they reside (in a one-to-one relationship), so that their clustering properties can be derived within the framework of the halo model developed by Mo & White (1996). Such models have been proved to be extremely useful in describing the clustering of high-redshift sources such as quasars, Lyman Break and SCUBA (Submillimetre Common-User Bolometer Array) galaxies (see, for example, Matarrese et al. 1997; Moscardini et al. 1998; Magliocchetti et al. 2001; Martini & Weinberg 2001; Porciani & Giavalisco 2002), where the assumption of one such object per halo can be considered a reasonable guess.

However, the validity of this approach breaks down as one moves to objects with higher number densities, such as low-redshift galaxies. The distribution of these kind of sources within dark matter haloes is, in general, an unknown quantity which will depend on the

*E-mail: maglio@sissa.it

efficiency of galaxy formation via some complicated physics connected to processes such as gas cooling and/or supernova feedback (see e.g. Somerville et al. 2001; Benson et al. 2001).

The analytical connection between the distribution of sources within dark matter haloes and their clustering properties has been studied in detail by a number of recent papers (Peacock & Smith 2000; Seljak 2000; Scoccimarro et al. 2001; Berlind & Weinberg 2002; Bullock, Wechsler & Somerville 2002; Marinoni & Hudson 2002; Moustakas & Somerville 2002; van den Bosch, Yang & Mo 2003; Yang, Mo & van den Bosch 2003; see also Cooray & Sheth 2002 for an extensive review on the topic) which mainly focus on the issue of the halo-occupation function, i.e. the probability distribution of the number of galaxies brighter than some luminosity threshold hosted by a virialized halo of given mass. Within this framework, the distribution of galaxies within haloes is shown to determine galaxy–galaxy clustering on small scales, being responsible for the observed power-law behaviour at separations $r \lesssim 3$ Mpc.

A number of parameters are necessary to describe the halo-occupation distribution (i.e. the probability of finding N_{gal} galaxies in a halo of mass m) of a class of galaxies. These parameters – expected to vary with galaxy type – cannot be worked out from first principles and have to rely for their determination either on comparisons with results from semi-analytical models or on statistical measurements coming from large data sets, with an obvious preference for this second approach.

The two last-generation 2dF Galaxy Redshift and Sloan Digital Sky Surveys (SDSS) (York et al. 2000; Colless et al. 2001) come to our help because – with their unprecedented precision in measuring galaxy clustering – they can, in principle, constrain the functional form of the halo-occupation distribution (see also Zehavi et al. 2003).

Lower-order clustering measurements, such as the spatial two-point correlation function, are already available for samples of 2dF sources (Norberg et al. 2002; Hawkins et al. 2003; Madgwick et al. 2003). In this work, we will use the results of Madgwick et al. (2003) on the clustering properties of late-type and early-type galaxies to investigate possible differences in the processes responsible for the birth and evolution of these two classes of sources.

The layout of the paper is as follows. Section 2 introduces the formalism necessary to describe galaxy clustering within the halo-occupation distribution context. Key ingredients for this kind of analysis are the average number $\langle N_{gal}\rangle(m)$ of galaxies hosted in dark matter haloes of mass m, a measure of the spread $\langle N_{gal}(N_{gal} - 1)\rangle(m)$ about this mean value and the spatial distribution $\rho(r)$ of galaxies within their haloes. In Section 3, we briefly describe the 2dF Galaxy Redshift Survey, with particular attention devoted to measurements of the luminosity function and correlation function for early-type (i.e. passively evolving) and late-type (which are still in the process of active star formation) galaxies, and derive estimates for the number density of these sources. Section 4 presents and discusses our results on the distribution of different types of galaxies within dark matter haloes as obtained by comparing predictions on their number density and correlation function with 2dF observations, whereas Section 5 summarizes our conclusions.

Unless differently stated, throughout this work we will assume that the density parameter $\Omega_0 = 0.3$, the vacuum energy density $\Lambda = 0.7$, the present-day value of the Hubble parameter (in units of 100 km s^{-1} Mpc^{-1}) $h_0 = 0.65$ and $\sigma_8 = 0.8$ (with σ_8 being the rms linear density fluctuation within a sphere with a radius of $8h^{-1}$ Mpc), as the latest results from the joint analysis of cosmic microwave background and 2dF data seem to indicate (see, for example, Lahav

et al. 2002; Spergel et al. 2003). Note, however, that the normalization of the linear power spectrum of density fluctuations is still very controversial: estimates of σ_8 from either weak-lensing or cluster abundances range between 0.6 and 1.0, whereas some analyses of galaxy clustering seem to favour values ~ 0.7 (van den Bosch, Mo & Yang 2003b). Our results will depend slightly on the assumed value for σ_8.

2 GALAXY CLUSTERING: THE THEORY

The purpose of this Section is to introduce the formalism and to specify the ingredients necessary to describe galaxy clustering at the two-point level. Our approach follows the one adopted by Scoccimarro et al. (2001), which is in turn based on the analysis performed by Scherrer & Bertschinger (1991). In this framework, the galaxy–galaxy correlation function can be written as

$$\xi_g(\mathbf{x} - \mathbf{x}') = \xi_g^{1h}(\mathbf{x} - \mathbf{x}') + \xi_g^{2h}(\mathbf{x} - \mathbf{x}'), \tag{1}$$

with

$$\begin{aligned}\xi_g^{1h} = \frac{1}{\bar{n}_g^2} \int n(m)\langle N_{gal}(N_{gal} - 1)\rangle(m)\, dm \\ \times \int \rho_m(\mathbf{y})\rho_m(\mathbf{y} + \mathbf{x} - \mathbf{x}')\, d^3 y,\end{aligned} \tag{2}$$

and

$$\begin{aligned}\xi_g^{2h} = \frac{1}{\bar{n}_g^2} \int n(m_1)\langle N_{gal}\rangle(m_1)\, dm_1 \\ \times \int n(m_2)\langle N_{gal}\rangle(m_2)\, dm_2 \int \rho_{m_1}(\mathbf{x} - \mathbf{x}_1)\, d^3 x_1 \\ \times \int \rho_{m_2}(\mathbf{x}' - \mathbf{x}_2)\xi(\mathbf{x}_1 - \mathbf{x}_2; m_1, m_2)\, d^3 x_2,\end{aligned} \tag{3}$$

where the first term ξ_g^{1h} accounts for pairs of galaxies residing within the same halo, whereas the term ξ_g^{2h} represents the contribution coming from galaxies in different haloes. Note that all the above quantities are dependent on the redshift z, even though we have not made it explicit.

In the above equations, $\langle N_{gal}\rangle(m)$ is the mean number of galaxies per halo of mass m, and $\langle N_{gal}(N_{gal} - 1)\rangle(m)$ – also dependent on the mass of the halo hosting the galaxies – is a measure of the spread about this mean value. The mean comoving number density of galaxies is defined as

$$\bar{n}_g = \int n(m)\langle N_{gal}\rangle(m)\, dm, \tag{4}$$

where $n(m)$ is the halo mass function which gives the number density of dark matter haloes per unit mass and volume. $\xi(\mathbf{x}_1 - \mathbf{x}_2; m_1, m_2)$ is the two-point cross-correlation function between haloes of mass m_1 and m_2; finally, $\rho_m(\mathbf{y})$ is the (spatial) density distribution of galaxies within the haloes, normalized so to obtain

$$\int_0^{r_{cut}} \rho_m(\mathbf{y})\, d^3 y = 1, \tag{5}$$

where r_{cut} is the radius which identifies the outer boundaries of the halo.

From the above discussion, it follows that, in order to work out ξ_g, we need to specify the halo–halo correlation function, the halo mass function, the spatial distribution of galaxies within the haloes and a functional form for the number distribution of galaxies within the haloes. This is done as follows.

2.1 Halo–halo correlation function

An approximate model for the two-point correlation function of dark matter haloes can be easily obtained from the mass autocorrelation function as (see, for example, Porciani & Giavalisco 2002)

$$\xi(\mathbf{r}, z, m_1, m_2)$$
$$= \begin{cases} \xi_{dm}(r, z)b_1(m_1, z)b_2(m_2, z) & \text{if } r \geqslant r_1 + r_2 \\ -1 & \text{otherwise,} \end{cases} \quad (6)$$

where the above expression takes into account the halo–halo spatial exclusion ($r_1 = r_{cut_1}$ and $r_2 = r_{cut_2}$ are the Eulerian radii of the collapsed haloes, in general identified with their virial radii), and the mass–mass correlation function $\xi_{dm}(r, z)$ – fully specified for a given cosmological model and a chosen normalization of σ_8 – has been calculated following the approach of Peacock & Dodds (1996), which is sufficiently accurate in both the linear and non-linear regimes. In fact, results obtained with the more precise algorithm developed by Smith et al. (2003) differ significantly from those obtained with the method by Peacock & Dodds (1996) only in the regime where the one-halo term dominates the two-point clustering signal.

Instead, the linear bias factor $b(m, z)$ of individual haloes of mass m at redshift z can be written as (Sheth & Tormen 1999; see also Cole & Kaiser 1989; Mo & White 1996; Catelan et al. 1997; Porciani et al. 1998)

$$b(m, z) = 1 + \frac{a\nu - 1}{\delta_c} + \frac{2p/\delta_c}{1 + (a\nu)^p}, \quad (7)$$

with $p = 0.3$, $a = 0.707$, $\nu = (\delta_c/\sigma)^2$, where $\delta_c \simeq 1.686$ and σ are the critical overdensity for collapse and the linear rms variance of the power spectrum on the mass-scale m at redshift z, respectively.

Note that, at variance with previous works (e.g. Peacock & Smith 2000; Seljak 2000; Berlind & Weinberg 2001; Scoccimarro et al. 2001) in which the halo–halo correlation function was derived only in the linear regime, our equation (6) fully accounts for the non-linear evolution of density fluctuations. Using linear theory to compute the two-halo term can be considered as a good approximation on large scales ($r \gtrsim 5$ Mpc), where the clustering growth is indeed still linear, and does not create any problems on small scales ($r \lesssim 1$ Mpc), where the one-halo term ξ_g^{1h} dominates the clustering signal. However, it breaks down at intermediate distances where the ξ_g^{1h} and ξ_g^{2h} contributions are of comparable importance. It follows that the use of a linear halo–halo correlation function in equation (3) leads systematically to a serious underestimate of the clustering signal (1) produced by low-z galaxies on scales $1 \lesssim r/[\text{Mpc}] \lesssim 5$, when compared with results obtained by taking into account the fully non-linear behaviour of $\xi_{dm}(r, z)$. For this reason, we believe our approach to be more consistent than the ones adopted so far. We note that similar models – unknown to us till the very last stages of the present paper – have also been used by Zehavi et al. (2003), Yang et al. (2003) and van den Bosch et al. (2003a).

2.2 Mass function

For the analytical expression of the halo mass function, we rely once again on the Sheth & Tormen (1999) form,

$$n(m, z) = \frac{A\bar{\rho}}{m^2}\sqrt{\frac{a\nu}{2\pi}}\left[1 + \frac{1}{(a\nu)^p}\right]\exp\left(-\frac{a\nu}{2}\right)\left|\frac{d(\ln\nu)}{d(\ln m)}\right| \quad (8)$$

(with $A = 0.322$, $\bar{\rho}$ the mean background density and the other quantities defined as above), because it gives an accurate fit to the results of N-body simulations with the same initial conditions (Jenkins et al. 2001; Sheth, Mo & Tormen 2001).

2.3 Spatial distribution of galaxies

The first, easiest approach one can take for the spatial distribution of galaxies within a halo of specified mass m is to assume that galaxies follow the dark matter profile. Under this hypothesis, we can then write

$$\rho'_m(r) = \rho_m(r)m = \bar{\rho}\frac{fc^3/3}{cr/r_{vir}(1 + cr/r_{vir})^2}, \quad (9)$$

where we use the Navarro, Frenk & White (1997, hereafter NFW) expression, which provides a good description of the density distribution within virialized haloes in numerical simulations. In equation (9), r_{vir} is the virial radius of the halo, related to its mass via $m = (4\pi r_{vir}^3/3)\Delta\bar{\rho}$, where Δ (=340 for an $\Omega = 0.3$ universe at $z = 0$) is the characteristic density contrast of virialized systems; $f = \Delta/[\ln(1+c)-c/(1+c)]$; and for the concentration parameter c, we use equations (9) and (13) in Bullock et al. (2001).

Clearly, the assumption for the distribution of galaxies within virialized haloes to trace the dark matter profile is not necessarily true. For instance, the semi-analytic models by Diaferio et al. (1999) suggest that this cannot hold for both late-type and early-type galaxies, because blue galaxies tend to reside in the outer regions of their parent haloes, whereas red galaxies are preferentially found near the halo centre.

For this reason, in the following analysis we will also consider spatial distributions of the form $\rho'_m(r) \propto (r/r_{vir})^{-\beta}$, with $\beta = 2$, 2.5, 3, where the first value corresponds to the singular isothermal sphere case.

The last remark concerns the choice for values of r_{cut} in equations (5) and (6). All the profiles (both the NFW and the power laws) considered so far formally extend to infinity, leading to divergent values for the associated masses. This implies the need to 'artificially' truncate the distribution profiles at some radius r_{cut}. One sensible choice is to set $r_{cut} \equiv r_{vir}$, because one expects galaxies to form within virialized regions, where the overdensity is greater than a certain threshold. However, this might not be the only possible choice since: for instance, as a consequence of halo–halo merging, galaxies might also be found in the outer regions of the newly formed halo, at a distance from the centre greater than r_{vir}.

The way different assumptions for the steepness of the profiles and different choices for r_{cut} affect the galaxy–galaxy correlation function on small scales ($r \lesssim 1$ Mpc) is presented in Fig. 1. To this particular aim, both ξ_g^{1h} and ξ_g^{2h} have been derived from equation (1) by setting $\langle N_{gal}\rangle = \langle N_{gal}(N_{gal} - 1)\rangle = 1$ for all halo masses greater than $10^{10.7}$ M$_\odot$, and 0 otherwise.

The two panels show the case for $r_{cut} = r_{vir}$ (top) and $r_{cut} = 2r_{vir}$ (bottom); solid, short-dashed, long–short-dashed and dotted lines represent the results for a NFW, a power law with $\beta = 2.5$, a power law with $\beta = 2$ and a power law with $\beta = 3$ distribution profiles, respectively. Lower curves (for $r \to 0$) correspond to the ξ_g^{2h} term (contribution from objects in different haloes), whereas the upper ones indicate the ξ_g^{1h} term.

As Fig. 1 shows clearly, both the scale at which the transition from a regime where objects in different haloes dominate the clustering signal to a regime where galaxies within the same halo start giving a contribution and also the amplitudes of the ξ_g^{1h} and ξ_g^{2h} terms depend greatly on the radius chosen to truncate the distribution profiles. In more detail, the amplitude of both terms decreases and differences between predictions obtained for different profiles become more pronounced as the value for r_{cut} increases. Finally note that – independently of the value of r_{cut} – a stronger clustering signal at small scales is expected, in general, for steeper density profiles.
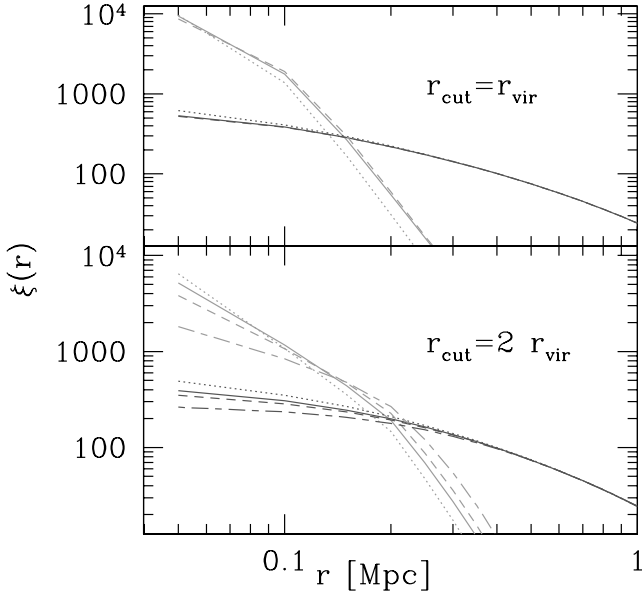
Figure 1. Results for the galaxy–galaxy correlation function as obtained from different assumptions for the galaxy distribution profiles $\rho(r)$ and different choices for r_{cut}. The case for $r_{cut} = r_{vir}$ is shown in the top panel, while the one for $r_{cut} = 2r_{vir}$ is presented in the bottom panel. Solid, short-dashed, long–short-dashed and dotted lines represent the predictions for a NFW, a power law with $\beta = 2.5$, a power law with $\beta = 2$ and power law with $\beta = 3$ distribution runs, respectively. Lower curves correspond to the term ξ_g^{2h} in equation (1) (contribution from objects in different haloes), whereas the upper ones indicate the ξ_g^{1h} term. All the above curves have been calculated by setting $\langle N_{gal}\rangle = \langle N_{gal}(N_{gal} - 1)\rangle = 1$ in equation (1) for all halo masses greater than $10^{10.7}$ M$_\odot$, and 0 otherwise.

Results originating from different assumptions for a spatial distribution of galaxies within dark matter haloes and different truncation radii will be investigated further in the following sections.

2.4 Halo-occupation function

A key ingredient in the study of the clustering properties of galaxies is their halo-occupation function $p(N_{gal}|m)$ which gives the probability for a halo of specified mass m to contain N_{gal} galaxies. In the most general case, $p(N_{gal}|m)$ is entirely specified by the knowledge of its n moments $\langle N_{gal}^n\rangle(m)$ which, in principle, can be determined observationally by means of the so-called 'counts in cells' analysis (see, for example, Benson 2001). Unfortunately, this is not feasible in reality, as measures of the higher moments of the galaxy distribution get extremely noisy for $n > 4$, even for two-dimensional catalogues [see, for example, Gaztanaga 1995, for an analysis of the Automatic Plate Mesuring (APM) survey].

A possible way to overcome this problem is to rely on the lower-order moments of the galaxy distribution to determine the low-order moments of the halo-occupation function, and then to assume a functional form for $p(N_{gal}|m)$ in order to work out all the higher moments (see, for example, Scoccimarro et al. 2001; Berlind & Weinberg 2002). Clearly, better and better determinations of $p(N_{gal}|m)$ are obtained as we manage to estimate higher and higher moments of the galaxy distribution function.

Since this work relies on measurements of the two-point correlation function of 2dF galaxies, equation (1) shows that in our case, only the first and second moment of the halo-occupation function

can be determined from the data, as these are the only two quantities which play roles in the theoretical description of ξ_g.

Following Scoccimarro et al. (2001), we chose to write the mean number of galaxies per halo of specified mass m as

$$\langle N_{gal}\rangle(m) = 0 \qquad \text{if } m < m_{cut}$$
$$\langle N_{gal}\rangle(m) = (m/m_0)^{\alpha_1} \qquad \text{if } m_{cut} \leqslant m < m_0$$
$$\langle N_{gal}\rangle(m) = (m/m_0)^{\alpha_2} \qquad \text{if } m \geqslant m_0, \tag{10}$$

where m_{cut}, m_0, α_1 and α_2 are parameters to be determined by comparison with observations. The choice of the above functional form for $\langle N_{gal}\rangle(m)$ relies on the physics connected with galaxy formation processes (see, for example, Benson et al. 2001; Sheth & Diaferio 2001; Somerville et al. 2001). For instance, m_{cut} gives the minimum mass of a halo able to host a galaxy because – for potential wells which are not deep enough – galaxy formation is inhibited by supernova processes occurring amongst the first stars which can blow the remaining gas away from the halo itself, therefore suppressing further star formation. On the other hand, given that the internal velocity dispersion of haloes increases with halo mass, gas is expected to cool less efficiently and therefore to inhibit galaxy formation at some level in more massive haloes. In a hierarchical scenario for structure formation, however, the most massive objects are formed by merging and accretion of smaller units. Thus, one expects the number of galaxies to increase with the halo size in the high-mass regime. Then all this can be parameterized by a broken power law of the form (10), with m_0 the 'threshold mass' at which the transition between the two different scaling laws occurs.

The last ingredient needed for the description of two-point galaxy clustering is the second moment of the halo-occupation function appearing in equation (1). This term quantifies the spread (or variance) about the mean value of the number counts of galaxies in a halo. A convenient parametrization for this quantity is

$$\langle N_{gal}(N_{gal} - 1)\rangle(m) = \alpha(m)^2\langle N_{gal}\rangle^2, \tag{11}$$

where $\alpha(m) = 0$, $\log(m/m_{cut})/\log(m_0/m_{cut})$ and 1 for $m < m_{cut}$, $m_{cut} \leqslant m < m_0$ and $m \geqslant m_0$, respectively. Note that, whereas the high-mass value for $\alpha(m)$ reflects simply Poissonian statistics, the functional form at intermediate masses (chosen to fit the results from semi-analytical models – see, for example Sheth & Diaferio 2001; Berlind & Weinberg 2002 – and smoothed particle hydrodynamics simulations – Berlind et al. 2003), describe the sub-Poissonian regime.

As a last consideration, note that equation (1) presents in both the ξ_g^{1h} and ξ_g^{2h} terms convolutions of density profiles. Because this is somehow difficult to deal with, we prefer to work in Fourier space, where all the expressions simply become multiplications over the Fourier transforms of the profiles. Therefore equation (1) is equivalent to

$$\bar{n}_g^2\Delta_g(k) = \int n(m)\langle N_{gal}(N_{gal} - 1)\rangle(m)|u_m(k)|^2\,dm$$
$$+ \int u_{m_1}(k)\langle N_{gal}\rangle(m_1)n(m_1)\,dm_1$$
$$\times \int u_{m_2}(k)n(m_2)\langle N_{gal}\rangle(m_2)\Delta(k, m_1, m_2)\,dm_2, \tag{12}$$

where – allowing for the exclusion effects, as in equation (6) – $\Delta(k, m_1, m_2) = \Delta_{dm}(k)b(m_1)b(m_2)$ is the power spectrum of haloes of mass m_1 and m_2; ($\Delta_{dm}(k) = k^3/(2\pi^2)P_{dm}(k)$ is the normalized nonlinear power spectrum for dark matter (see, for example, Peacock

& Dodds 1996);

$$u_m(k) = \frac{k^3}{(2\pi^2)} \int_0^{r_{cut}} \rho_m(r) \frac{\sin(kr)}{kr} 4\pi r^2 \, dr, \tag{13}$$

with $\rho_m(r)$ defined as in (5), is the Fourier transform of the galaxy distribution profile truncated at r_{cut}; and where all the quantities are taken implicitly at a fixed z. In this framework, the galaxy–galaxy correlation function can then be obtained from equation (12) via

$$\xi_g(r) = \int \Delta_g(k) \frac{\sin(kr)}{kr} \frac{dk}{k}. \tag{14}$$

3 THE 2dF GALAXY REDSHIFT SURVEY

The 2dF Galaxy Redshift Survey (2dFGRS; Colless et al. 2001) is a large-scale survey aimed at obtaining spectra for 250 000 galaxies to an extinction-corrected limit for completeness of $b_J = 19.45$ over an area of 2151 deg². The survey geometry consists of two broad declination strips: a larger one in the South Galactic Pole, covering the area $3^h30^m \lesssim$ RA(2000) $\lesssim 21^h40^m$, $-37.5° \lesssim$ Dec.(2000) $\lesssim -22.5°$, and a smaller one set in the North Galactic Pole, with $9^h50^m \lesssim$ RA(2000) $\lesssim 14^h50^m$, $2.5° \lesssim$ dec(2000) $\lesssim -7.5°$, plus 100 random two-degree fields spread uniformly over the 7000 deg² of the APM catalogue in the southern Galactic hemisphere.

The input catalogue for the survey is a revised version of the APM galaxy catalogue (Maddox et al. 1990a; Maddox, Efstathiou & Sutherland 1990b, 1996) which includes over 5 million galaxies down to $b_J = 20.5$. Redshifts for all the sources brighter than $b_J = 19.45$ are determined in two independent ways, via both cross-correlation of the spectra with specified absorption-line templates (Colless et al. 2001) and by emission-line fitting. These automatic redshift estimates have been confirmed subsequently by visual inspection of each spectrum, and the more reliable of the two results is chosen as the final redshift. A quality flag was assigned to each redshift: $Q = 3, 4$ and 5 correspond to reliable redshift determination, $Q = 2$ means a probable redshift and $Q = 1$ indicates no redshift measurement. The success rate in redshift acquisition for the surveyed galaxies (determined by the inclusion in the 2dF sample of only those objects with quality flags $Q = 3–5$) is estimated about 95 per cent (Folkes et al. 1999). The median redshift of the galaxies is 0.11 and the great majority of them have $z < 0.3$.

3.1 Luminosity functions and number densities

Madgwick et al. (2002) calculate the optical b_j luminosity function (LF) for different subsets of $M - 5 \log_{10}(h_0) \leqslant -13$ 2dFGRS galaxies defined by their spectral type. The spectral classification – based upon a Principal Component Analysis – was performed for 75 589 galaxies found at redshifts $0.01 < z < 0.15$ and allowed to divide the whole population into four well-defined classes according to the strength of their star-formation activity: from type 1 (early-type galaxies only showing absorption lines in their spectra) to type 4 (extremely active star-forming galaxies).

Fitting functions for the different luminosity distributions are presented in Madgwick et al. (2002) and can be used to determine the average number density of galaxies of different spectral types via (see e.g. Lin et al. 1996)

$$\bar{n}_{g_i} = N_i \times \left[\int_{z_{min}}^{z_{max}} S_i(z)(dV/dz) \, dz \right]^{-1}, \tag{15}$$

with the selection function $S_i(z)$ defined as

$$S_i(z) = \frac{\int_{\max[M_{min}^i(z), M_{min}]}^{\min[M_{max}^i(z), M_{max}]} \Phi_i(M) \, dM}{\int_{M_{min}}^{M_{max}} \Phi_i(M) \, dM}, \tag{16}$$

where dV/dz is the volume element, $i = 1, 2, 3, 4$ refers to the spectral class, N_i is the total number of galaxies belonging to a specific type found in the survey and Φ_i is their luminosity function. $M_{min} = -13 + 5 \log_{10}(h_0)$, $z_{min} = 0.01$ and $M_{max} \simeq -21 + 5 \log_{10}(h_0)$, $z_{max} = 0.15$ are the respective minimum and maximum absolute magnitudes and redshifts of the objects under examination, whereas $M_{min(max)}^i(z) = b_{max(min)} - 25 - 5 \log(d_L^i) - k_i(z)$, where $k_i(z)$ is the K-correction, d_L^i is the luminosity distand $b_{min} = 14$, $b_{max} = 19.45$ are the apparent magnitude limits of the 2dF survey.

Then we applied equation (15) to the four different galaxy types and found

$$\bar{n}_{g_1} = 9.6 \times 10^{-3} \begin{cases} -4.4 \times 10^{-3} \\ +7.0 \times 10^{-2} \end{cases}$$

$$\bar{n}_{g_2} = 0.0103 \pm 3 \times 10^{-4}$$

$$\bar{n}_{g_3} = 0.015 \begin{cases} -8 \times 10^{-4} \\ +9 \times 10^{-4} \end{cases} \tag{17}$$

$$\bar{n}_{g_4} = 0.018 \pm 1.8 \times 10^{-3},$$

where the quoted 1σ errors, in all but the type 1 case, are obtained by varying the 'break' luminosities M_i^* and the faint-end slopes μ_i of the Schechter functions $\Phi_i(M) = (0.4 \ln 10)\Phi_i^*[10^{-0.4(M-M_i^*)}]^{1+\mu_i} \exp[-10^{-0.4(M-M_i^*)}]$ (note that our calculations are independent of the normalizations Φ_i^*) along their joint 1σ error ellipse.

Two features have to be noticed in (17). First, errors in $\bar{n}_{g_1}$ – especially the upper 1σ limit of the number density – are significantly larger than those derived for the other three classes of sources. This is due to the fact that the Schechter function might not provide a good fit to the faint end of the LF of type 1 galaxies (Madgwick et al. 2002); an extra term of the form $\Phi(M) = 10^{a+bM}$ is needed for $M - 5 \log_{10}(h_0) \gtrsim -16$, where the parameters a and b can only be determined from the data with quite large uncertainties. Because it is the faint end of the LF which mostly contributes to the determination of $\bar{n}_{g_1}$, and because this is the region where the errors on a and b dominate over those derived for the various parameters in the Schechter function, this explains our finding for such large uncertainties associated to the measurement of $\bar{n}_{g_1}$.

The second point to be noticed concerns the errors associated to $\bar{n}_{g_4}$. In fact, it turns out that, also in the case of type 4 galaxies, the Schechter function does not provide a good fit to the faint end of the luminosity function as it overestimates the number density of $M - \log_{10}(h_0) \gtrsim -16$ galaxies systematically. This implies that the total number of type 4 sources as derived from integration of the LF is in agreement with the observed one only if we subtract from the best estimate $\bar{n}_{g_4}$ in equation (17) an error corresponding to a 3σ confidence level in μ_4. Because – as we will see better in the next section – the observed number density of galaxies plays a relevant role in the determination of the best halo-occupation model, we have decided in the case of type 4 sources to consider errors on μ_4 at the 3σ level; this propagates to a lower limit for $\bar{n}_{g_4} = 0.0127$.

Finally, from the luminosity function, we can also determine another quantity which will be useful in the following sections: the effective redshift of a class of sources defined as $z_i^{eff} = \int_{z_{min}}^{z_{max}} z S_i(z)(dV/dz) \, dz$. Numbers obtained for the different types of galaxies under examination then read $z_1^{eff} = 0.098$, $z_2^{eff} = 0.091$,

$z_3^{\mathrm{eff}} = 0.082$, $z_4^{\mathrm{eff}} = 0.078$, indicating a preference for late-type galaxies to be found at lower redshifts than early-type objects.

3.2 Correlation functions

A sample with the same selection criteria as the one introduced in Section 3.1 but containing more (96 791) objects has been used by Madgwick et al. (2003) to calculate the clustering properties of galaxies belonging to different spectral types. In order to increase the statistics associated to the measurements, galaxies have been grouped into two broad categories: early-type (36 318 objects with effective redshift 0.1, to be identified with those sources belonging to spectral class 1) and late-type (60473 objects with effective redshift 0.09, obtained by taking into account all galaxies from spectral classes 2 3 and 4).

The different observed correlation functions are shown in Figs 2 and 6 for early-type and late-type galaxies, respectively. In order to get rid of redshift distortions, the correlation function in real space has been inferred by computing the bi-dimensional correlation parallel and transverse to the line-of-sight, $\xi_{\mathrm{g}}(r_P, r_T)$, and by integrating it in the r_P direction. Therefore, the quantity presented in Figs 2 and 3 corresponds to

$$\bar{\xi}_{\mathrm{g}}(r_T) = 2 \int_{r_T}^{\infty} \xi_{\mathrm{g}}(r) \frac{r\,\mathrm{d}r}{(r^2 - r_T^2)^{1/2}}. \tag{18}$$

Error bars have been obtained by bootstrap resampling, adapting the method presented by Porciani & Giavalisco (2002).

Measurements for the integrated correlation function (18) differ for the two populations not only in their amplitude, but also in the slopes (by fitting the data with a power law $\xi(r) = (r/r_0)^{\gamma}$, Madgwick et al. 2003 find $r_0 = 3.67 \pm 0.30\,h^{-1}$ Mpc, $\gamma = 1.60 \pm 0.04$ for late-type galaxies and $r_0 = 6.10 \pm 0.34\,h^{-1}$ Mpc, $\gamma = 1.95$
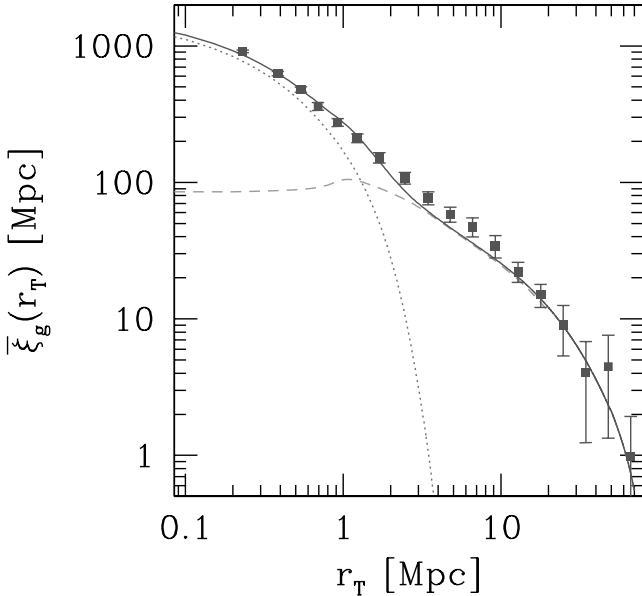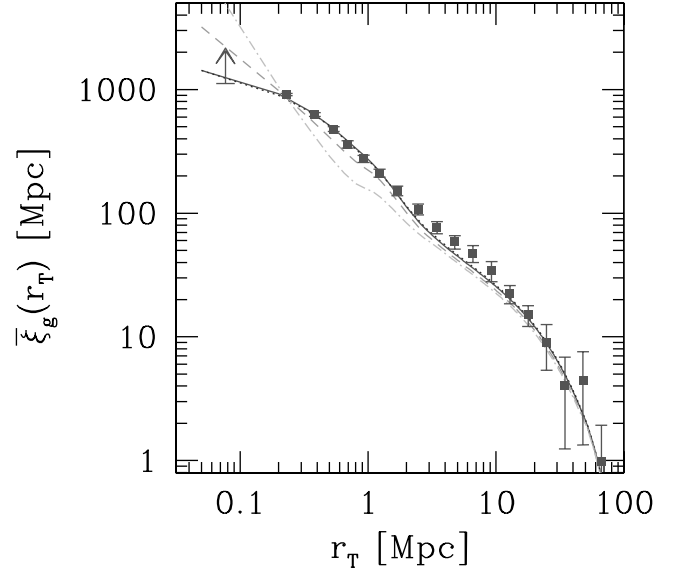

Figure 3. Projected correlation function of early-type galaxies. Data points represent the results from Madgwick et al. (2003), whereas solid, dashed, dotted and dash–dotted curves illustrate the best-fitting models obtained for a NFW, a power law with $\beta = 2.5$, a power law with $\beta = 2$ and a power law with $\beta = 3$ galaxy distribution profiles, respectively (see text for details). The arrow shows the lower limit to the measured correlation function set on small scales by fibre collisions in the 2dF survey (Hawkins, private communication).

± 0.03 for early-type sources). As we will see extensively in the following sections, these differences can provide a great amount of information on the processes associated to galaxy formation in the two different cases of passive and active star-forming galaxies.

4 RESULTS

In order to determine the best values for the parameters describing the halo-occupation number (10) we allowed them to vary within the following region:

$$-1 \leqslant \alpha_1 \leqslant 2;$$
$$-1 \leqslant \alpha_2 \leqslant 2;$$
$$10^9\,\mathrm{M}_{\odot} \leqslant m_{\mathrm{cut}} \leqslant 10^{13}\,\mathrm{M}_{\odot};$$
$$m_{\mathrm{cut}} \leqslant m_0 \leqslant 10^3\,m_{\mathrm{cut}}.$$

Combinations of these four quantities have then been used to evaluate the mean number density of galaxies $\bar{n}_{\mathrm{g}}$ via equation (4). Only values for $\bar{n}_{\mathrm{g}}$ within 2σ from the observed ones (quoted in Section 3.1) were accepted, and the corresponding values for α_1, α_2, m_{cut} and m_0 have been subsequently plugged into equation (1) to produce – for a specified choice of the distribution profile and effective redshift z^{eff} (slightly different in the case of early-type and late-type galaxies) – the predicted galaxy–galaxy correlation function, to be integrated via equation (18) and to be compared with the data by means of a least-squares (χ^2) fit.

The value for the truncation radius of the halo was set to r_{vir} and the above procedure was repeated for different choices of $\rho_m(r)$. The following subsections describe the results obtained for the two different classes of early- and late-type galaxies.

Figure 2. Projected correlation function of early-type galaxies. Data points represent the results from Madgwick et al. (2003), whereas the solid curve is the best fit to the measurements obtained for a halo number density of the form (10), with $\alpha_1 = -0.2$, $\alpha_2 = 1.1$, $m_{\mathrm{cut}} = 10^{12.6}$ M$_{\odot}$, $m_0 = 10^{13.5}$ M$_{\odot}$ and for galaxies distributed within their dark matter haloes according to a NFW profile. Dashed and dotted lines indicate the contribution $\xi_{\mathrm{g}}^{2\mathrm{h}}$ from galaxies residing in different haloes and the $\xi_{\mathrm{g}}^{1\mathrm{h}}$ term originating from galaxies within the same halo, respectively.

Table 1. Best-fitting values for the parameters describing the halo-occupation number (10), expressed for different choices of the distribution profile and truncation radius. PL2, PL2.5 and PL3 correspond to profiles described by power laws with slopes $\beta = 2$, $\beta = 2.5$ and $\beta = 3$, respectively. Errors are for a 68.3 per cent confidence level and three degrees of freedom. $\bar{n}_g$ (in Mpc^{-3}) and b are the average number density of sources and the bias on large scales, as derived from the combination of the best-fitting parameters associated to each model. All the masses are measured in M$_\odot$ units. Vanishing error bars mean that either the best-fitting value lies on the boundary of the sampled parameter space (for example, when $\alpha_1 = -1$) or that the uncertainty is smaller than our grid step (0.1 for all parameters).

	NFW	PL2	PL2.5	PL3
EARLY-TYPE				
$r_{\rm cut} = r_{\rm vir}$	$\chi^2_{\rm min} = 4.0$	$\chi^2_{\rm min} = 4.9$	$\chi^2_{\rm min} = 13.2$	$\chi^2_{\rm min} = 68.9$
	$\alpha_1 = -0.2^{+0.6}_{-0.5}$	$\alpha_1 = -0.5^{+1.0}_{-0.3}$	$\alpha_1 = -0.6^{+0.7}_{-0.4}$	$\alpha_1 = -0.5^{+0.1}_{-0.5}$
	$\alpha_2 = 1.1^{+0.1}_{-0.2}$	$\alpha_2 = 1.0^{+0.1}_{-0.1}$	$\alpha_2 = 1.5^{+0.0}_{-0.2}$	$\alpha_2 = 1.8^{+0.0}_{-0.6}$
	$\mathrm{Log}[m_{\rm cut}] = 12.6^{+0.1}_{-0.5}$	$\mathrm{Log}[m_{\rm cut}] = 12.7^{+0.0}_{-0.7}$	$\mathrm{Log}[m_{\rm cut}] = 12.7^{+0.2}_{-0.4}$	$\mathrm{Log}[m_{\rm cut}] = 12.7^{+0.2}_{-0.2}$
	$\mathrm{Log}[m_0] = 13.5^{+0.0}_{-0.5}$	$\mathrm{Log}[m_0] = 13.4^{+0.1}_{-0.4}$	$\mathrm{Log}[m_0] = 13.7^{+0.1}_{-0.3}$	$\mathrm{Log}[m_0] = 13.9^{+0.1}_{-0.4}$
	$n_g = 8.4 \times 10^{-4}$	$n_g = 8.6 \times 10^{-4}$	$n_g = 1.31 \times 10^{-3}$	$n_g = 1.34 \times 10^{-3}$
	b = 1.33	b = 1.34	b = 1.31	b = 1.30
LATE-TYPE				
$r_{\rm cut} = r_{\rm vir}$	$\chi^2_{\rm min} = 90.4$	$\chi^2_{\rm min} = 107.6$	$\chi^2_{\rm min} = 81.7$	$\chi^2_{\rm min} = 38.8$
$r_{\rm cut} = 2r_{\rm vir}$	$\chi^2_{\rm min} = 9.7$	$\chi^2_{\rm min} = 7.2$	$\chi^2_{\rm min} = 10.7$	$\chi^2_{\rm min} = 14.4$
	$\alpha_1 = -0.4^{+2.4}_{-0.6}$	$\alpha_1 = -1.0^{+3.0}_{-0.0}$	$\alpha_1 = -0.6^{+2.4}_{-0.4}$	$\alpha_1 = -0.7^{+2.7}_{-0.3}$
	$\alpha_2 = 0.7^{+0.1}_{-0.1}$	$\alpha_2 = 0.7^{+0.2}_{-0.1}$	$\alpha_2 = 0.7^{+0.3}_{-0.1}$	$\alpha_2 = 0.6^{+0.3}_{-0.1}$
	$\mathrm{Log}[m_{\rm cut}] = 11.0^{+0.2}_{-1.8}$	$\mathrm{Log}[m_{\rm cut}] = 11.1^{+0.1}_{-1.9}$	$\mathrm{Log}[m_{\rm cut}] = 11.0^{+0.3}_{-1.8}$	$\mathrm{Log}[m_{\rm cut}] = 11.0^{+0.3}_{-1.8}$
	$\mathrm{Log}[m_0] = 11.4^{+0.6}_{-0.4}$	$\mathrm{Log}[m_0] = 11.4^{+0.5}_{-0.3}$	$\mathrm{Log}[m_0] = 11.4^{+0.8}_{-0.4}$	$\mathrm{Log}[m_0] = 11.4^{+0.8}_{-0.4}$
	$n_g = 0.032$	$n_g = 0.031$	$n_g = 0.034$	$n_g = 0.035$
	b = 0.98	b = 0.99	b = 0.97	b = 0.97

4.1 Early-type galaxies

The best description of the data in this case is provided by a model with $\alpha_1 \simeq -0.2$, $\alpha_2 \simeq 1.1$, $m_{\rm cut} = 10^{12.6}$ M$_\odot$, $m_0 = 10^{13.5}$ M$_\odot$ [in good agreement with the findings of Zehavi et al. (2003)] and with a mild preference for galaxies to be distributed within their dark matter haloes according to a NFW profile. The projected galaxy–galaxy correlation function for this combination of values and the NFW spatial distribution is illustrated by the solid curve in Fig. 2, whereas the dashed and dotted lines indicate the contribution ξ_g^{2h} from galaxies residing in different haloes and the ξ_g^{1h} term originating from galaxies within the same halo, respectively. The agreement between data and predictions is good at all scales, even though the model tends to underestimate the correlation function at intermediate scales (between 3 and 10 Mpc), where the maximum discrepancy is ~20 per cent.

A more quantitative assessment of the goodness of the match can be found in Table 1, which – for each choice of the distribution profile $\rho_m(r)$ and for the different classes of early-type and late-type galaxies – provides the value of the $\chi^2 = \chi^2_{\rm min}$ obtained for the best fit to the data and also the corresponding estimates for the parameters which appear in the description of the halo-occupation number (10). 1σ errors on these quantities are obtained by requiring their different combinations not to produce models for the galaxy–galaxy correlation function which – when compared to the measurements – correspond to χ^2 values which differ from the minimum by a factor greater than $\Delta\chi^2 = 3.53$, where this last figure has been derived for an analysis with three degrees of freedom (assuming Gaussian errors). Three is, in fact, the number of degrees obtained if one subtracts from the number of independent $\bar{\xi}_g$ measurements (eight; Madgwick, private communication)[1] the number of parameters to determine (four) and the constraint on $\bar{n}_g$ (one).

A closer look to Table 1 shows that, in the case of early-type galaxies, the best-fitting values for the parameters appearing in equation (10) are independent – except for the most extreme cases of very poor fits – of the particular choice for the spatial distribution of galaxies within the haloes. This is verified even though different profiles are associated to different values for $\chi^2_{\rm min}$, and is due to the fact that, while quantities such as $\langle N_{\rm gal} \rangle$ and $\langle N^2_{\rm gal} \rangle$ (and therefore the parameters associated to them) mainly determine the amplitudes of the ξ_g^{1h} and ξ_g^{2h} terms, the distribution of galaxies within the haloes is directly responsible for the slope of ξ_g, especially on scales $r \lesssim 1$ Mpc.

This effect is better seen in Fig. 3, which presents the best-fitting models obtained for different choices of the distribution run. In more detail, the solid line is for a NFW profile, the dotted line is for a power-law profile with $\beta = 2$, the dashed line is for a power-law profile with $\beta = 2.5$ and the dashed-dotted line represents the case of a power-law profile with $\beta = 3$. Even though all the curves are almost indistinguishable from each other on all scales $r \gtrsim 2$ Mpc due to the very similar best-fitting values obtained for the parameters which describe $\langle N_{\rm gal} \rangle$ and $\langle N_{\rm gal}(N_{\rm gal} - 1) \rangle$, this does not hold any longer at smaller distances. In fact, when we push the analysis inside the haloes, the profile assumes a crucial importance; for instance, in the case of early-type galaxies, it is clear that whereas profiles such as NFW and singular isothermal sphere can provide a good fit to the observations (with a slight preference for the first model), anything steeper than these two is ruled out drastically by the data because they do not exhibit enough power on scales $0.3 \lesssim r/[\mathrm{Mpc}] \lesssim 2$.

Table 1 states the same conclusion from a more quantitative point of view, showing that, although the NFW profile provides the best description of the data and the value of $\chi^2_{\rm min}$ for a $\beta = 2$ model is still within the 1σ range of the acceptable fits (for Gaussian errors), profiles of the power-law form with $\beta \gtrsim 2.5$ are too steep

[1] It is in some sense arbitrary to decide how many principal components of the correlated errors correspond to a real signal and how many correspond

to noise. This can be done, for instance, by considering a fixed fraction of the variance (see, for example, Porciani & Giavalisco 2002).
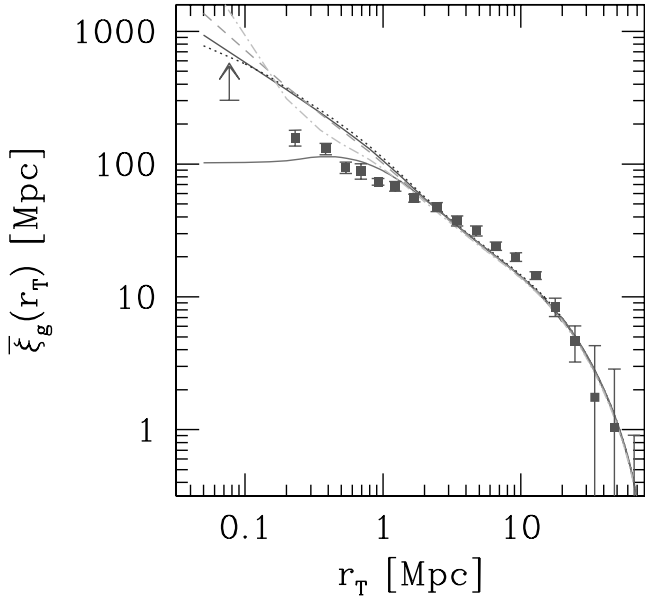
Figure 4. Projected correlation function of late-type galaxies. Data points represent the results from Madgwick et al. (2003), whereas solid, dashed, dotted and dash–dotted curves illustrate the best-fitting models obtained for a NFW, a power law with $\beta = 2.5$, a power law with $\beta = 2$ and a power law with $\beta = 3$ galaxy distribution profiles and for a truncation radius $r_{cut} = r_{vir}$, respectively. The curve flattening around $r \lesssim 0.5$ Mpc illustrates the contribution ξ_g^{2h} from galaxies residing in different haloes (see text for details). The arrow shows the lower limit to the measured correlation function set on small scales by fibre collisions in the 2dF survey (Hawkins, private communication).

to be accepted as satisfactory descriptions of the observed galaxy correlation function. We remark once again that, because the spatial distribution of galaxies within haloes of specified mass and their mean number and variance affect different regions of the observed correlation function, these two effects are untangled so that there is no degeneracy in the determination of $\langle N_{gal} \rangle$ and $\rho(r)$ preferred by the data.

Because different profiles lead to notably different predictions for the correlation function on increasingly smaller ($r \lesssim 0.2$ Mpc, see Fig. 3) scales, one would, in principle, like to be able to explore this region in order to put stronger constraints on the distribution of galaxies within their haloes. Unfortunately, this cannot be done because – as Hawkins et al. (2003) have shown – fibre collisions in the 2dF survey can decrease the measured $\xi_g(r)$ significantly on scales $r \lesssim 0.1$ Mpc, leading to systematic underestimates. Nevertheless, one can still use the 2dF measurements of the correlation function as a lower limit to the real galaxy–galaxy clustering strength, to be compared with predictions stemming from different density runs. This is done in Fig. 3, where the arrow represents the 2dF measurement of the early-type correlation function on a scale $r \simeq 0.07$ Mpc. In this particular case, all the models appear to have enough power on such small scales, as none of them falls below the accepted range of variability of the measured $\xi_g(r)$. Therefore, on the basis of the present data, we cannot break the degeneracy between NFW and PL2 profiles as to which one can provide the best description of the data in the whole r range.

If we then concentrate our attention on the two distribution profiles that can correctly reproduce the observations (NFW and power law with $\beta = 2$, hereafter PL2) and analyse the best-fitting values obtained for the parameters describing the halo-occupation number

and their associated errors, we find for instance that, whereas the slope α_2 – which determines the increment of the number of sources hosted by dark matter haloes of increasing mass in the high-mass regime – is very well determined, the situation is more uncertain for what concerns α_1, counterpart of α_2 in the low-mass regime. On the other hand, m_{cut} and m_0 exhibit errors of similar magnitudes, with upper limits better determined than the lower ones, this last effect possibly due to the constraints on $\bar{n}_g$, which discard every model not able to produce enough galaxies, as is the case for high values of m_{cut} and m_0.

An analysis of the χ^2 hypersurface also shows that all the parameters but α_2 (and especially m_{cut} and m_0) are covariant. This means that, in order to be consistent with the available data, decreasing m_{cut} with respect to its best-fitting value implies lowering m_0 and increasing α_1. The interplay is probably due to the fact that both α_1 and m_{cut} only play a role in the low-mass regime which affects mainly the intermediate-to-large scale regions of the galaxy correlation function, where measurements are more dominated by uncertainties. Conversely, ξ_g on small scales is strongly dependent on the adopted value of α_2, therefore making this last quantity measurable with an extremely high degree of precision.

4.2 Late-type galaxies

The case for late-type galaxies appears more tricky to treat in the framework of our analysis due to the shallow slope of the observed correlation function (see Section 3.2). In fact, as can be appreciated in Fig. 4, no model can describe the slow rise of the data correctly on scales $r \lesssim 2$ Mpc, even though the large-scale normalization of all the curves reproduces the measured one with a good approximation. This is shown in a more quantitative way in Table 1, which quotes the minimum χ^2 values obtained for different distribution profiles
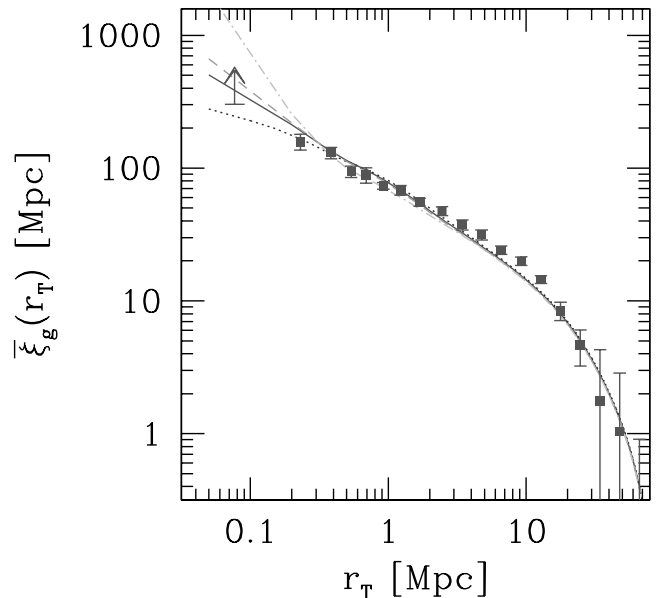

Figure 5. Projected correlation function of late-type galaxies. Data points represent the results from Madgwick et al. (2003), whereas solid, dashed, dotted and dash–dotted curves illustrate the best-fitting models obtained for a NFW, a power law with $\beta = 2.5$, a power law with $\beta = 2$ and a power law with $\beta = 3$ galaxy distribution profiles and for a truncation radius $r_{cut} = 2 \cdot r_{vir}$, respectively. The arrow shows the lower limit to the measured correlation function set on small scales by fibre collisions in the 2dF survey (Hawkins, private communication).

and a truncation radius $r_{cut} = r_{vir}$: no model gives an acceptable fit and the corresponding figures for χ^2_{min} are around 39, in the best case.

A closer look at Fig. 4 indicates that the problem has to be connected with the excess of power on intermediate scales exhibited by the ξ^{2h}_g contribution of pairs of galaxies from different haloes (the solid curve which flattens on scales ∼0.5 Mpc), which creates the mismatch between the observed slope and the steeper 'best-fitting models'. In other words, what the plot reveals is that, in the model, there are too many pairs of galaxies coming from different haloes at distances $0.5 \lesssim r/[Mpc] \lesssim 2$ with respect to what the data seem to indicate.

Therefore a possible way out is to deprive the intermediate-scale region of pairs of objects residing in different haloes. This can be done if one assumes that the distribution of late-type galaxies associated to a given halo does not vanish at the virial radius, but extends to some larger distance. Then the mutual spatial exclusion of haloes ensures that there will be no pairs of galaxies belonging to different haloes in the desired range. Indeed, it is not surprising to find S0 and disc galaxies futher away than a virial radius from a cluster centre (see, for example, fig. 8 in Domínguez, Muriel & Lambas 2001). We can attempt to let the galaxy distribution extend to, say, two virial radii. As Fig. 5 shows, this assumption reduces the discrepancy between models and measurements greatly: the theoretical curves now have the right slope and amplitude on scales $0.5 \lesssim r/[Mpc] \lesssim 2$, and the corresponding best fits to the data exhibit χ^2_{min} values which are (almost) as good as in the case of early-type galaxies (see Table 1). Note that, even though we adopted a somehow ad hoc procedure to find a better description of the measurements, our finding seems to point out to the well-known phenomenon of

morphological segregation (see, for example, Adami, Biviano & Mazure 1998; Domínguez et al. 2001; Giuricin et al. 2001; Madgwick et al. 2003 for some recent results), whereby late-type galaxies tend to be found in the outer regions of groups and clusters, whereas early-type ones sink preferentially into the group or cluster centre. A simple calculation in fact shows that, for scales $0.5 \lesssim r/[Mpc] \lesssim 2$, haloes which in our model are required to host star-forming galaxies up to two virial radii have masses in the range $10^{11.9} \lesssim m/M_\odot \lesssim 10^{13.7}$. As we will see better in the next section, haloes within this mass range are expected to host on average $3 \lesssim \langle N_{gal} \rangle \lesssim 50$ late-type galaxies, limits which span from a small group to a cluster of galaxies.

Therefore, our result does not contradict the well-established fact that galaxies form within the virialized regions of dark matter haloes (i.e. at a distance $< r_{vir}$ from their centre). What it states simply is that – possibly due to merging processes and accreting flows – late-type galaxies in groups and clusters are found within their dark matter haloes up to distances from the centre corresponding to about two virial radii. Note that we are not claiming that these galaxies are slingshot towards their final position during the merging event. The key idea is that, at a certain point in the process of approaching a merging event, galaxies residing in the progenitors of a given halo will be associated with the final object itself as their host haloes lose their identity by the formation of high density 'bridges' which alter the output of cluster-finding algorithms like the friends-of-friends one (on which both our mass function and bias parameters are based). This phenomenon might be less important for the population of early-type galaxies, which probably form in galaxy mergers that tend to be more concentrated within their host haloes.

Now we discuss the results on the halo-occupation number and distribution profile obtained for the population of late-type galaxies under the assumption of a truncation radius corresponding to two virial radii. As Table 1 shows, the best fit to the data in this case is provided by a model with $\alpha_1 \simeq -1$, $\alpha_2 = 0.7$, $m_{cut} = 10^{11.1}$ $M_\odot$, $m_0 = 10^{11.4}$ $M_\odot$ and for galaxies distributed within their dark matter haloes according to a PL2 profile, even though on the basis of this analysis we cannot really discard any $\rho(r)$ model apart from PL3 because they all show χ^2_{min} values within 1σ from the favourite one (as for early-type galaxies, a model is accepted as a fair description of the data if the corresponding χ^2_{min} lie within $\Delta\chi^2 = 3.53$ from the best fit).

In order to shed some more light on the distribution profiles able to describe the correlation function of star-forming galaxies correctly, we have adopted the same approach as in the previous subsection and used the lowest r_T ($\simeq$0.07 Mpc) measurement of $\xi_g(r)$ derived by the 2dF team for late-type objects (Hawkins, private communication) as a lower limit to the true galaxy clustering strength, to be compared with the available models. This is done in Fig. 5, where the lowest-scale data is represented by the vertical arrow. At variance with the case of early-type galaxies, the singular isothermal sphere model – even though providing the best fit to the $r \gtrsim 0.1$ Mpc data – is now ruled out by the behaviour of the observed correlation function, which needs steeper profiles in this regime. On the basis of the above comparison, one then has that only the PL2.5 and NFW density runs can still be accepted as reasonable descriptions of the data, with a slightly stronger preference given to the latter model because it also provides the (second) best fit to the observations on scales $r > 0.1$ Mpc.

The projected galaxy correlation function originating from the combination of values given in Table 1 and the NFW profile is illustrated by the solid curve in Fig. 6. The dashed and dotted lines indicate the contribution ξ^{2h}_g from galaxies hosted in different haloes
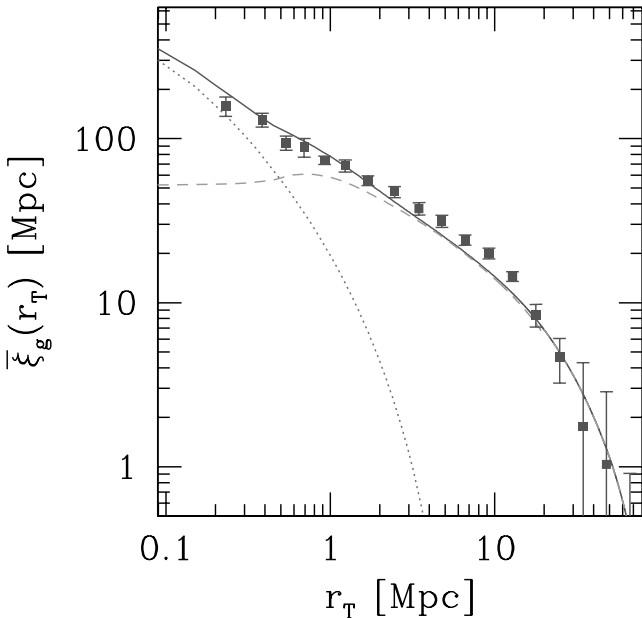

Figure 6. Projected correlation function of late-type galaxies. Data points represent the results from Madgwick et al. (2003), whereas the solid curve is the best fit to the measurements obtained for a halo number density of the form (10), with $\alpha_1 = -0.4$, $\alpha_2 = 0.7$, $m_{cut} = 10^{11}$ $M_\odot$, $m_0 = 10^{11.4}$ $M_\odot$ and for galaxies distributed within their dark matter haloes according to a NFW profile with $r_{cut} = 2r_{vir}$. Dashed and dotted lines indicate the contribution ξ^{2h}_g from galaxies residing in different haloes and the ξ^{1h}_g term originating from galaxies within the same halo, respectively.

and the ξ_g^{1h} term given by galaxies residing within the same halo, respectively. Note that, as in Fig. 2, our best-fitting models tend to underestimate the observed correlation at intermediate scales (between 5 and 15 Mpc) by $\sim$20 per cent.

The uncertainties associated to the parameters describing the low-mass regime of the halo-occupation number seem to be bigger than those found for passive galaxies. However, this result is misleading, because the larger errors quoted for α_1 and which are associated to the 1σ lower limit of m_{cut} reflect only the fact that the low-mass regime in equation (10) is practically non-existent for star-forming galaxies as $m_0 \simeq m_{cut}$. In this case, one then has that the halo-occupation number behaves as the pure power law: $\langle N_{gal}\rangle(m) = (m/m_0)^{\alpha_2}$ at almost all mass-scales, where both α_2 and m_0 are very well constrained.

As it was in the case of early-type galaxies, an analysis of the χ^2 hypersurface helps us to understand the interplay between the different parameters describing the halo-occupation number. We find that, whereas α_2 and m_0 show little variability, α_1 and m_{cut} are strongly covariant, with higher values for the former quantity corresponding to lower minimum masses associated to haloes able to host a star-forming galaxy.

As a final remark, we note that – also for late-type galaxies – values for α_1, α_2, m_{cut} and m_0 which provide the best fit to the data do not depend on the particular form adopted for the spatial distribution of galaxies within the haloes. Once again, this finding stresses the absence of degeneracy in the determination of quantities such as $\rho(r)$ and the average number of galaxies in haloes of specified mass, $\langle N_{gal}\rangle(m)$: as long as one can rely on clustering measurements which probe the inner parts of dark matter haloes, both functional forms can be obtained with no degree of confusion from the same data set.

4.3 Scatter of the halo-occupation distribution and number density profiles

All our results for the galaxy density profiles are derived by assuming a specific functional form for $\langle N_{gal}(N_{gal}-1)\rangle(m)$, as given in equation (11). In principle, this could bias our determination of the spatial distribution of galaxies within a single halo (Berlind & Weinberg 2002). In order to understand the importance of this effect, we repeated the analysis of the correlation functions by assuming three different functional forms for the second moment of the halo distribution function. In particular, we took $\alpha = 1, 0.3, 0.1$ in equation (11), independent of the halo mass. We found that none of these models can fit the data as well as our original prescription. However, for purely Poissonian scatter, the best-fitting models for late-type galaxies are almost identical to our fiducial models, and the ranking of the density profiles does not change. On the other hand, for early-type galaxies, Poissonian models are associated with large values of χ^2 (23.7 at best, for PL2) due to the overabundance of power on small scales (the favourite values for m_{cut} and m_0 are typically $\sim$10 times smaller than in our fiducial case) but, again, only the PL2 and NFW profiles are acceptable. When the scatter instead is strongly sub-Poissonian ($\alpha = 0.1, 0.3$), we find that it is practically impossible to get a good description of $\bar{\xi}_g$. In fact, in this case, the one-halo term in the correlation function is heavily depressed and one is forced to increase the value of α_2 and m_{cut} to try to match the data. Anyway, all the models are unacceptable due to lack of power on small scales, and all the profiles are associated with nearly the same values of χ^2. In summary, even though we confirm the presence of some degeneracy between the second moment of the halo-occupation distribution
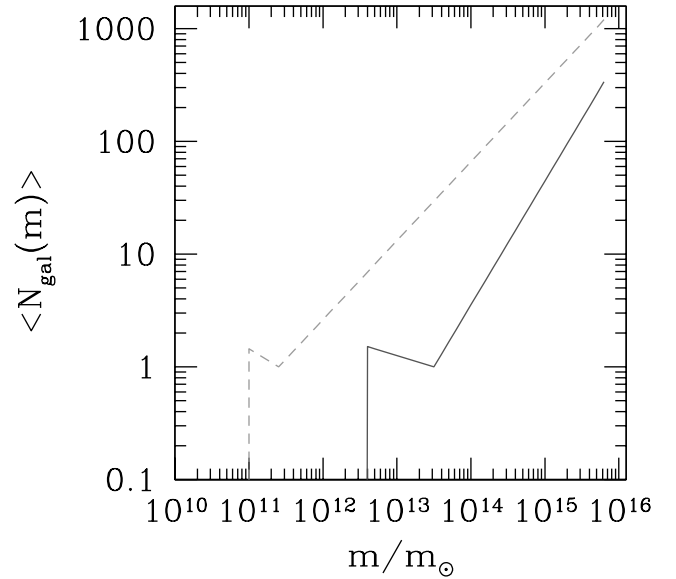

Figure 7. Average number of galaxies $\langle N_{gal}(m)\rangle$ per dark matter halo of specified mass m (expressed in $M_\odot$ units). The solid line represents the case for early-type galaxies, whereas the dashed line is for late-type objects.

and the profile of the galaxy distribution, as discussed in Berlind & Weinberg (2002), we find that it is extremely hard to find models that can give accurate description of the data. This means that the apparent freedom in assuming a functional form for $\langle N_{gal}(N_{gal}-1)\rangle(m)$ is not actually so. As a consequence of this, we are led to believe that our conclusions regarding the density profiles of 2dF galaxies are indicative of a real trend, even though they are indeed drawn in the framework of a specific model.

5 THE GALAXY MASS FUNCTION

The results derived in the previous sections allow us to draw some conclusions on the intrinsic nature of galaxies of different types. Fig. 7 shows the average number of galaxies per dark matter halo of specified mass m, as obtained from the best fits to the clustering measurements of Madgwick et al. (2003). The dashed line describes the case for star-forming galaxies, whereas the solid line is for early-type objects.

Late-type galaxies are found in haloes with masses greater than $\sim10^{11} M_\odot$ (even though this figure, especially in its lower limit, is not determined with a great accuracy, given the interplay between m_{cut} and α_1), and their number increases with the mass of the halo which hosts them according to a power law (except in the limited region $10^{11.0} \leqslant m/M_\odot < 10^{11.4}$) with slope $\alpha_2 = 0.7$ and normalization $1/m_0 = 10^{-11.4} M_\odot^{-1}$.

Instead, early-type galaxies start appearing within haloes of noticeably higher masses, $m \gtrsim 10^{12.6} M_\odot$. In the low-mass region (i.e. for $m \lesssim 10^{13.5} M_\odot$), the data seems to indicate that each halo is populated by approximately one passive galaxy on average, even though results in this mass range are affected by some uncertainties. More solid are the findings in the high-mass ($m \gtrsim 10^{13.5} M_\odot$) regime, which show $\langle N_{gal}\rangle$ to increase with halo mass as a power law of slope $\alpha_2 \simeq 1.1$, steeper than what found for the population of late-type galaxies. Then one has that the average number of star-forming galaxies within a halo does not increase with its mass as fast as it happens for passive galaxies, even though late-type objects are found to dominate the 2dF counts at all mass-scales.

This result seems in disagreement with the observational evidence that early-type galaxies are found preferentially in clusters, whereas star-forming galaxies reside mainly in relatively underdense regions. However, the discrepancy is only apparent because, whereas in the Madgwick et al. (2003) analysis the population of early-type galaxies is a homogeneous sample, the class of late-type galaxies includes any object which has some hint of star formation activity in its spectrum (see Section 3). This implies that anything – from highly irregular and star-bursting galaxies to S0 types – will be part of the star-forming sample. Then the lack of a characteristic mass for the transition from haloes populated mainly by late-type galaxies to haloes inhabited principally by passive objects finds a natural explanation if one considers that S0 galaxies – also found preferentially in groups and clusters – are, in this case, associated to the population of late-type objects, making up for about 35 per cent of the sample (Madgwick et al. 2002). We also reiterate that both the 2dF and its parent APM surveys select sources in the blue (b_j) band, therefore creating a bias in favour of star-forming galaxies which are more visible than passively evolving ellipticals in this wavelength range.

It is interesting to compare our results with those by van den Bosch et al. (2003a), who used 2dF data to estimate the conditional luminosity functions of early- and late-type galaxies. They combined their results to obtain the mean halo-occupation number of galaxies in given absolute-magnitude ranges. Since our analysis is based on an apparent-magnitude limited sample, this complicates the comparison. For their faintest late-type galaxies, the behaviour of $\langle N_{\mathrm{gal}} \rangle (m)$ is relatively similar to our findings, with a cut-off below $\sim 10^{11}$ M$_\odot$, a small decrement up to $10^{11.5}$ M$_\odot$ and a power-law regime d $\log \langle N_{\mathrm{gal}} \rangle (m)/$d $\log m \simeq 0.6$ for larger masses. As for early-type galaxies, results are in good agreement with ours, with a power-law high-mass regime with slope d $\log \langle N_{\mathrm{gal}} \rangle (m)/$d $\log m \simeq 1$. However, van den Bosch et al. (2003a) find a less sharp cut-off at small masses, with $\log(m_0/\mathrm{M_\odot}) \sim 12.5$ and $\langle N_{\mathrm{gal}}(m) \rangle$ declining gently with decreasing m up to $10^{10.5-11}$ M$_\odot$. Given all the systematic uncertainties belonging to the two methods of analysis, the similarity of the results is remarkable, confirming the potential of the halo-occupation distribution method.

Finally, Fig. 8 shows the 'galaxy mass function', i.e. the number density of galaxies per unit of dark matter mass and volume as obtained by multiplying the average number of galaxies found in a halo of specified mass $\langle N_{\mathrm{gal}}(m) \rangle$ by the halo mass function (8). Again, the solid curve identifies the case for early-type galaxies, whereas the dashed one is derived for the population of star-forming galaxies. The dotted line indicates the Sheth & Tormen (1999) halo mass function (8).

6 CONCLUSIONS

Results from Madgwick et al. (2002, 2003) on the correlation function and luminosity function of $\sim 96\,000$ 2dFGRS galaxies with $0.01 < z < 0.15$ have been used to investigate some of the properties of early- and late-type galaxies, such as the so-called halo-occupation number $\langle N_{\mathrm{gal}} \rangle$ (i.e. the mean number of sources that populate a halo of given mass m) and the spatial distribution of such galaxies within their dark matter haloes.

In order to perform our analysis, we have considered four distribution profiles: three power laws of the form $\rho(r) \propto r^{-\beta}$ with $\beta = 2, 2.5, 3$ and a NFW profile chosen to mimic the assumption for galaxies within haloes to trace the distribution of dark matter. As a first approximation, all the profiles have been truncated at the halo virial radius.
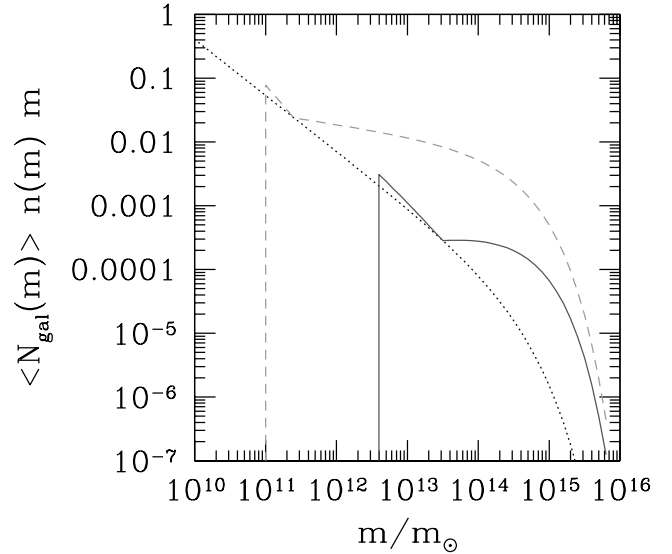

Figure 8. Number of galaxies per unit of (log) dark matter mass and volume (in Mpc^{-3} units). The solid line represents the result for early-type galaxies, whereas the dashed line is for late-type objects. For comparison, the dotted line indicates the Sheth & Tormen (1999) mass function $n(m)$ of dark matter haloes.

For consistency with results from semi-analytical models (see e.g. Benson et al. 2001), the halo-occupation number was parametrized by a broken power law of the form $(m/m_0)^{\alpha_1}$ in the low mass regime $m_{\mathrm{cut}} \leqslant m \leqslant m_0$ and $(m/m_0)^{\alpha_2}$ at higher masses, where m_{cut} is the minimum mass of a halo that can host a galaxy.

The resulting theoretical average number density $\bar{n}_{\mathrm{g}}$ and galaxy–galaxy correlation function – sum of the two terms $\xi_{\mathrm{g}}^{\mathrm{1h}}$, representing the contribution from galaxies residing within the same halo, and $\xi_{\mathrm{g}}^{\mathrm{2h}}$, which considers pairs belonging to different haloes – have then been compared with the observations in order to determine those models which provide the best description of the data, both in the case of late-type and early-type galaxies. Note that, at variance with previous works which only considered a linear $\xi_{\mathrm{g}}^{\mathrm{2h}}$, our analysis provides a full treatment for non-linearity and also includes the assumption of halo–halo spatial exclusion, in a way that makes the model entirely self-consistent.

The main conclusions are as follows.

(i) Early-type galaxies are well described by a halo-occupation number of the form broken power law (10) with $\alpha_1 \simeq -0.2$, $\alpha_2 \simeq 1.1$, $m_{\mathrm{cut}} \simeq 10^{12.6}$ M$_\odot$ and $m_0 \simeq 10^{13.5}$ M$_\odot$, where the two quantities which determine the intermediate-to-high mass behaviour of $\langle N_{\mathrm{gal}} \rangle$ are measured with a good accuracy.

(ii) No model can provide a reasonable fit to the correlation function of late-type galaxies, because they all show an excess of power with respect to the data on scales $0.5 \lesssim r/[\mathrm{Mpc}] \lesssim 2$. In order to obtain an acceptable description of the observations, one has to assume that star-forming galaxies are distributed within haloes of masses comparable to those of groups and clusters up to two virial radii. This result is consistent with the phenomenon of morphological segregation, whereby late-type galaxies are found mostly in the outer regions of groups or clusters (extending well beyond their virial radii), whereas passive objects sink preferentially into their centres.

(iii) With the above result in mind, one finds that late-type galaxies can be described by a halo-occupation number of the single power-law form with $\alpha_2 \simeq 0.7$, $m_{\mathrm{cut}} \simeq 10^{11}$ M$_\odot$ and $m_0 \simeq$

$10^{11.4}$ M$_\odot$, where the quantities which describe $\langle N_{gal} \rangle$ in the high-mass regime are determined with a high degree of accuracy.

(iv) Within the framework of our models, galaxies of any kind seem to follow the underlying distribution of dark matter within haloes, as they present the same degree of spatial concentration. In fact, the data indicates both early-type and late-type galaxies to be distributed within their host haloes according to NFW profiles. However, we note that even though early-type galaxies can also be described by means of a shallower distribution of the form $\rho(r) \propto r^{-2}$, this cannot be accepted as a fair modelling of the data in the case of late-type galaxies, which allow for somehow steeper ($\beta \simeq$ 2.5) profiles instead. In no case can a $\beta = 3$ density run provide an acceptable description of the observed correlation function. These conclusions depend somehow on assuming a specific functional form for the second moment of the halo-occupation distribution. We showed, however, that there is not much freedom in the choice of this function if one wants to match the observational data accurately.

An interesting point to note is that results on the spatial distribution of galaxies within haloes and on their halo-occupation number are independent from each other. There is no degeneracy in the determination of $\langle N_{gal} \rangle$ and $\rho(r)$ as they dominate the behaviour of the two-point correlation function ξ_g at different scales. In fact, different distribution profiles principally determine the slope of ξ_g on small enough ($r \lesssim 1$ Mpc) scales which probe the inner regions of the haloes, whereas the halo-occupation number is mainly responsible for the overall normalization of ξ_g and for its slope on large-to-intermediate scales.

Our analysis shows that late-type galaxies can be hosted in haloes with masses smaller than is the case for early-type objects. This is probably due to the fact that early-type galaxies are on average more massive (where the term here refers to stellar mass) than star-forming objects, especially if one considers the population of irregulars, and points to a relationship between stellar mass of galaxies and mass of the dark matter haloes which host them.

The population of star-forming galaxies is found to be the dominant one at all mass-scales, a result that can be reconciliated with the well-established observational fact that early-type galaxies are found preferentially in clusters, while star-forming galaxies reside mainly in relatively underdense regions, by considering that about a third of the class of late-type sources in our sample is made of S0 galaxies, which are also found preferentially in groups and clusters. We also stress that both the 2dF and its parent APM surveys select sources in the blue band, therefore creating a bias in favour of star-forming galaxies which are more visible than passively evolving ellipticals in this wavelength range.

As a final remark, we note that the results of this work are partially biased by the need to assume a pre-defined functional form for both the halo-occupation number and the variance about this quantity. High-precision measurements of higher moments of the galaxy distribution function (for example, the skewness and the kurtosis) are of crucial importance if one wants to determine the distribution of galaxies within dark matter haloes in a non-parametric way, i.e. without the necessity to rely on any a priori assumption. In the near future, results from the 2dF and SSDS galaxy redshift surveys should be able to fill this gap.

REFERENCES

Adami C., Biviano A., Mazure A., 1998, A&A, 331, 439
Benson A. J., 2001, MNRAS, 325, 1039
Benson A. J., Cole S., Frenk C. S., Baugh C. M., Lacey C. G., 2001, MNRAS, 327, 1041
Berlind A. A., Weinberg D. H., 2002, ApJ, 575, 587
Berlind A. A. et al., 2003, ApJ, 593, 1
Bullock J. S., Wechsler R. H., Somerville R. S., 2002, MNRAS, 329, 246
Bullock J. S., Kolatt T. S., Sigad Y., Somerville R. S., Kravtsov A. V., Klypin A. A., Primack J. R., Dekel A., 2001, ApJ, 321, 559
Catelan P., Lucchin F., Matarrese S., Porciani C., 1997, MNRAS, 297, 692
Cole S., Kaiser N., 1989, MNRAS, 237, 1127
Colless M. et al., (2dFGRS team), 2001, MNRAS, 328, 1039
Cooray A., Sheth R., 2002, Phys. Rep., 372, 1
Diaferio A., Kauffmann G., Colberg J. M., White S. D. M., 1999, MNRAS, 307, 537
Domínguez M., Muriel H., Lambas D. G., 2001, ApJ, 121, 1266
Folkes S. R. et al., 1999, MNRAS, 308, 459
Gaztanaga E., 1995, MNRAS, 454, 561
Giuricin G., Samurovic S., Girardi M., Mezzetti M., Marinoni C., 2001, ApJ, 554, 857
Guzzo L., Strauss M. A., Fisher K. B., Giavanelli R., Haynes M. P., 1997, ApJ, 489, 37
Hawkins E. et al. (the 2dFGRS Team), 2003, MNRAS, submitted (astro-ph/0212375)
Jenkins A. et al. (the VIRGO Consortium), 1998, ApJ, 499, 20
Jenkins A., Frenk C. S., White S. D. M., Colberg J. M., Cole S., Evrard A. E., Couchman H. M. P., Yoshida N., 2001, MNRAS, 321, 372
Lahav O. et al. (2dFGRS Team), 2002, MNRAS, 333, 961
Lin H., Kirshner R. P., Shectman S. A., Landy S. D., Oemler A., Tucker D. L., Schechter P. L., 1996, ApJ, 464, 60
Loveday J., Maddox S. J., Efstathiou G., Peterson B. A., 1995, ApJ, 442, 457
Loveday J., Tresse L., Maddox S. J., 1999, MNRAS, 310, 281
Maddox S. J., Efstathiou G., Sutherland W. J., Loveday J., 1990a, MNRAS, 243, 692
Maddox S. J., Efstathiou G., Sutherland W. J., 1990b, MNRAS, 246, 433
Maddox S. J., Efstathiou G., Sutherland W. J., 1996, MNRAS, 283, 1227
Madgwick D. S. et al. (the 2dFGRS 2 Team), 2002, MNRAS, 333, 133
Madgwick D. S. et al. (the 2dFGRS 2 Team), 2003, MNRAS, 344, 847
Magliocchetti M., Bagla J., Maddox S. J., Lahav O., 2000, MNRAS, 314, 546
Magliocchetti M., Moscardini L., Panuzzo P., Granato G. L., De Zotti G., Danese L., 2001, MNRAS, 325, 1553
Marinoni C., Hudson M. J., 2002, ApJ, 569, 101
Martini P., Weinberg D. H., 2001, ApJ, 547, 12
Matarrese S., Coles P., Lucchin F., Moscardini L., 1997, MNRAS, 286, 115
Mo H. J., White S. D. M., 1996, MNRAS, 282, 347
Moscardini L., Coles P., Lucchin F., Matarrese S., 1998, MNRAS, 299, 95
Moustakas L., Somerville R. S., 2002, ApJ, 577, 1
Navarro J. F., Frenk C. S., White S. D. M., 1997, ApJ, 490, 493
Norberg P. et al. (the 2dFGRS 2 Team), 2002, MNRAS, 332, 827
Peacock J. A., Dodds S. J., 1996, MNRAS, 267, 1020
Peacock J. A., Smith R. E., 2000, MNRAS, 318, 1144
Porciani C., Giavalisco M., 2002, ApJ, 565, 24
Porciani C., Matarrese S., Lucchin F., Catelan P., 1998, MNRAS, 298, 1097
Scherrer R. J., Bertschinger E., 1991, ApJ, 381, 349
Scoccimarro R., Sheth R. K., Hui L., Jain B., 2001, ApJ, 546, 20
Seljak U., 2000, MNRAS, 318, 203

Sheth R. K., Tormen G., 1999, MNRAS, 308, 119

Sheth R. K., Diaferio A., 2001, MNRAS, 322, 901

Sheth R. K., Mo H. J., Tormen G., 2001, MNRAS, 323, 1

Smith R. C. et al., 2003, MNRAS, 341, 1311

Somerville R. S., Lemson G., Sigad Y., Dekel A., Kauffmann G., White S. D. M., 2001, MNRAS, 320, 289

Spergel D. M. et al., 2003, (astro-ph/0302209)

van den Bosch F. C., Yang X., Mo H. J., 2003a, MNRAS, 340, 771

van den Bosch F. C., Mo H. J., Yang X., 2003b, (astro-ph/0301104)

Yang X., Mo H. J., Jing Y. P., van den Bosch F. C., Chu Y., 2003, MNRAS, submitted (astro-ph/0303524)

York D. G., Anderson J. E., Anderson S. F., Annis J., Bachall N. A., Bakken J. A. et al., 2000, AJ, 120, 1579

Zehavi et al. (the SDSS Collaboration), 2003, (astro-ph/0301280)

This paper has been typeset from a TEX/LATEX file prepared by the author.